Effects of different doses of X-ray irradiation on cell apoptosis, cell cycle, DNA damage repair and glycolysis in HeLa cells

HONG ZHAO[1-4*], YAFEI ZHUANG[1-3*], RUIBIN LI[1-3], YINYIN LIU[1-3], ZIJIE MEI[1,2], ZHONGSHI HE[1-3], FUXIANG ZHOU[2,3] and YUNFENG ZHOU[2,3]

[1]Hubei Key Laboratory of Tumor Biological Behaviors; [2]Department of Radiation and Medical Oncology and [3]Hubei Cancer Clinical Study Center, Zhongnan Hospital Affiliated to Wuhan University, Wuhan, Hubei 430071; [4]Department of Radiation Oncology, Shandong Academy of Medical Science, Shandong Cancer Hospital Affiliated to Shandong University, Jinan, Shangdong 250117, P.R. China

Received January 20, 2017; Accepted August 30, 2018

DOI: 10.3892/ol.2018.9566

Abstract. The present study examined the radiation biological response of cancer cells to different fractional irradiation doses and investigates the optimal fractional irradiation dose with improved biological effects. Radiobiological studies were performed at the molecular and cellular levels to provide insights into DNA damage and repair, and the apoptosis mechanism of cells that were exposed to different doses of X-ray irradiation (0, 2, 4, 6, 8, 10, 12.5, 15 and 20 Gy). Evidence of increased reactive oxygen species (ROS), DNA double strand breaks (DSB), cellular apoptosis, G2/M phase proportion and inhibition of cell proliferation were observed following irradiation. Differences in the ROS amount and apoptotic percentages of cells between the 2 and 4 Gy groups were insignificant. Compared with 0 Gy, the expression of the apoptosis suppression protein B-cell lymphoma-2 was decreased following at increased irradiation doses. However, apoptosis-associated protein Bcl-2-associated X (Bax), caspase-9 and BH3 interacting domain death agonist (Bid) were elevated following irradiation, compared with the control group (0 Gy). Furthermore, the expression levels of Bax in the 6, 8, 10 and 12.5 Gy groups were significantly increased, compared with the other groups. Caspase-9 expression with 2, 4, 6 and 8 Gy were increased compared with other groups, and the Bid levels with 6 and 8 Gy were also increased compared with other groups. G2/M phase arrest was associated with the increase of checkpoint kinase 1 and reduction of cyclin dependent kinase 1. DNA damage repair was associated with the protein Ku70 in the 2, 8, 10, 12.5, 15 and 20 Gy groups were less than other group. Compared with other group, Ku80 levels were reduced in the 6 and 8 Gy groups, and Rad51 levels were reduced in the 2, 8 and 10 Gy groups. The expression of hypoxia inducible factor-1α, c-Myc and glucose transporter 1 (GLUT1) demonstrated an increasing trend following irradiation in a dose-dependent manner, but the expression of pyruvate kinase M2, in the 2-10 Gy irradiation groups, and GLUT1, in the 12.5, 15 and 20 Gy irradiation groups, were reduced, compared with the other groups. Considering the DNA damage repair and apoptosis mechanisms at molecular and cellular levels, it was concluded that 2, 6, 8 and 10 Gy may be the optimal fractional dose that can promote cell apoptosis, and inhibit DNA damage repair and glycolysis.

Introduction

Radiation therapy serves an important role in the treatment of cancer, with almost half of all patients with cancer receiving radiotherapy in different stages of their disease. Since the 1930s, conventionally fractionated radiotherapy (CFRT) has been used for clinical therapy, with the implemented scheme being 1.8-2.0 Gy/fraction. CFRT exploits inherent differences between normal and tumor tissues. Tumor cells require increased energy for proliferation, while normal cells retain the ability to repair DNA injuries. The therapeutic benefit of CFRT was first explained by Bergonie and Tribondeau (1). Administering small daily doses of irradiation is key in CFRT, even if it damages tumor and normal tissues. Compared with normal tissues, tumor tissues have a reduced capability of repairing DNA damage caused by radiation. Over the course of a number of treatments, tumor tissues sustain increased cumulative damage, compared with normal tissues (2).

Toxicity of radiotherapy to normal cells limits the dose of radiation used. Over the past decades, there have been technical improvements to radiation therapy, in order to reduce the toxic effects of radiotherapy (2). Stereotactic Body Radiation Therapy (SBRT), as a novel cancer treatment strategy, accurately provides high doses of radiation to tumor tissues, while

Correspondence to: Professor Yunfeng Zhou or Professor Fuxiang Zhou, Department of Radiation and Medical Oncology, Zhongnan Hospital Affiliated to Wuhan University, 169 Donghu Road, Wuhan, Hubei 430071, P.R. China
E-mail: yfzhouwhu@163.com
E-mail: happyzhoufx@sina.com

*Contributed equally

Key words: fractional dose, irradiation, HeLa cells, DNA damage repair, apoptosis, glycolysis

reducing the exposure of surrounding tissues to toxic levels of radiation (2,3). Thus, a single high dose of radiation may be used in radiotherapy (4,5). SBRT, as an emerging cancer treatment strategy, has evolved in the late twentieth century. Unlike CFRT, SBRT utilizes ultra-high doses per fraction in treatment, generally in the range of 10-20 Gy/fraction, potentially exposing tumor and normal structures to the high-dose radiation (6-9). SBRT may have risk of treatment-associated complications while achieving increased rates of local control. Exposure to the high-dose radiation can irreversibly damage tumor and normal tissues and irreversible damage to normal tissue can seriously affect the body's function (2,10). Thus, not all patients who need radiation are suitable for this technique.

The present study investigated the cellular changes in cancer cells following irradiation at different doses. The aim was to observe the biological effects of different radiation doses on tumor cells, and this may provide theoretical support for selecting radiation fractional doses with superior biological effects. To determine the radiobiological responses of cancer cells following different radiation fractional doses and the optimal fractional radiation dose, radiobiological studies were performed at molecular and cellular levels to provide insights into DNA damage and repair, and the apoptosis mechanism of cells irradiated at doses between 0 and 20 Gy. Further elucidation of the cellular effects of different doses of radiation may contribute to the rationale for selecting the optimal fractional dose of radiation for cancer radiotherapy.

Materials and methods

Cell culture. HeLa cells obtained from the American Type Culture Collection (Manassas, VA, USA) were cultured in Dulbecco's modified Eagle's medium containing 10% fetal bovine serum (both from Gibco; Thermo Fisher Scientific, Inc., Waltham, MA, USA). Cell cultures were stored at 37˚C in an atmosphere containing 5% CO_2 in a humidified incubator. Cells used for each experiment were grouped according to the dose of irradiation (0, 2, 4, 6, 8, 10, 12.5, 15 and 20 Gy).

X-irradiation. X-irradiation experiments were performed at the Irradiation Facility of Zhongnan Hospital of Wuhan University (Wuhan, China). The medium was replaced prior to irradiation in a horizontal position. Cells were divided into different groups and exposed under (0, 2, 4, 6, 8, 10, 12.5, 15 and 20 Gy) X-rays separately with a Siemens Primus Accelerator machine (6 Mv; Siemens AG, Munich, Germany).

Cell Counting Kit-8 (CCK-8) assay for cell proliferation. CCK-8 reagent (Dojindo Molecular Technologies, Inc., Kumamoto, Japan) was used to determine the proliferation rate of cells, the cells was grouped according to the dose of irradiation (0, 2, 4, 6, 8, 10, 12.5, 15 and 20 Gy). The seeded ($1x10^4$ cells/well in 96-well plates) serum-starved cells were exposed to different doses of radiation (0, 2, 4, 6, 8, 10, 12.5, 15 and 20 Gy). Cells were washed using PBS prior to detection, then CCK-8 solution was added (10 μl CCK-8 and 90 μl Dulbecco's modified Eagle's medium without any supplements). At 3 h following the addition of CCK-8, the absorbance at 450 nm was measured at 24, 48, 72, 96 and 120 h followimg irradiation of cells in each group (0, 2, 4, 6, 8, 10, 12.5, 15 and 20 Gy) by micro-tablet reader (Microplate Reader, Sunrise, Tecan). The cell proliferation rates were calculated and the optical density value from the first day was used for normalization.

Immunocytochemistry for phosphorylated histone H2AX (γ-H2AX). Cells were plated and grown on coverslips ($5x10^4$ cells/well), 12 h after cells were seeded, a series of dose irradiation was performed as aforementioned (0, 2, 4, 6, 8, 10, 12.5, 15 and 20 Gy). At 20 min following irradiation, cells were fixed in 5% paraformaldehyde (Merck KGaA, Darmstadt, Germany) for 30 min at room temperature, then washed with PBS and permeabilized in 0.5% Triton (Sigma-Aldrich; Merck KGaA) for 10 min at room temperature. The cells were treated with the blocking fluid (5% bovine serum albumin, cat. no. SBJ-1239; NanJing SenBeiJia Biotechnology Co. Ltd., Nanjing, China) for 1 h at room temperature, then washed with PBS. The cells were subsequently probed with mouse anti-γ-H2AX antibody (ser139) (1:200 dilution; cat. no. 05-636-AF488; EMD Millipore, Billerica, MA, USA) and incubated overnight at 4˚C. The cells were then washed with PBS, stained with fluorescein isothiocyanate (FITC)-conjugated goat anti-rabbit secondary antibody (1:500 dilution; cat. no. 31635; Invitrogen; Thermo Fisher Scientific, Inc.) for 2 h at room temperature. All antibody dilutions were prepared in 5% bovine serum albumin (cat. no. SBJ-1239; NanJing SenBeiJia Biotechnology Co. Ltd.). Subsequently, three washing steps were performed with PBS, following which a cover glass was incubated with propidium iodide (PI) for 20 min at room temperature. Finally, images were captured with a fluorescence microscope (Nikon E-600; Nikon Corporation, Tokyo Japan) using a 1.3 aperture plan fluor x40 numerical aperture oil objective.

Cell cycle analysis. Cells were collected at 0, 6, 12, 18, 24, 30, 36, 42 and 48 h after irradiation by trypsinization purification at room temperature. Considering that there may be adherent cells, the supernatants and PBS used in washing steps were retained. Samples were fixed in cold 70% EtOH solution at 4˚C for 24 h. Cells were then washed with PBS two times, then stained with 500 μl PI solution (50 μg/ml PI and 1% RNase A; Sigma-Aldrich; Merck KGaA) for 50 min at 37˚C. Samples were measured immediately by flow cytometry (Accuri C6, BD Biosciences, San Jose, CA, USA). PI fluorescence of a minimum of $1x10^4$ cells was measured. Cells in the G0/G1, S and G2/M phases were determined followed filtering for doublets and aggregates. Doublets were filtered based on a FSC-A vs. FSC-H dot plot with BD Accuri C6 software version 1.0.202.1 (BD Biosciences).

Detection of apoptosis by Annexin V. During apoptotic cell detection, $1x10^5$ cells were inoculated in the 6-well culture plate and cultured for 12 h prior to irradiation, at 37˚C in an atmosphere containing 5% CO_2 in a humidified incubator. Cells were harvested at 48 and 72 h after irradiation at room temperature, then the cells were re-suspended in 100 μl staining buffer (PBS, cat. no. SH30256.01B; GE Healthcare Life Sciences, Hyclone, Logan, UT, USA) with 5 μl Annexin V-FITC (BD Pharmingen; BD Biosciences) and stained at room temperature for 15 min, followed by a quick staining

with 1 μg/ml PI (cat. no. P4864; Sigma-Aldrich; Merck KGaA) at room temperature for 10 min. The samples were analyzed on a LSRII flow cytometer (BD Biosciences). The data was then analyzed using Flow Jo software version 9.6.2 (FlowJo LLC, Ashland, OR, USA).

Mitochondrial membrane potential analysis. The JC-1 kit (Beyotime Institute of Biotechnology, Haimen, China) was used to detect the mitochondrial membrane potentials. Cell suspensions at $1x10^5$ cells/ml were cultured on glass cover-slips for 12 h at 37˚C in an atmosphere containing 5% CO_2 in a humidified incubator. At 6 h after irradiation, the cells were incubated with Dulbecco's PBS (DPBS) which was provided in the JC-1 kit and 1 μl JC-1 reagent at 37˚C for 15 min. Subsequently, the cells were washed with DPBS three times. The mitochondrial membrane potential was detected under a fluorescence microscope (x100 magnifications, Nikon E-600). The reduction in red fluorescence and the increase in green fluorescence indicated a decrease in the mitochondrial membrane potential.

Microscopic analysis of dihydroethidium (DHE) oxidation [reactive oxygen species (ROS) production] in cells. With the use of a 12-well plate, cells were plated at a density of $5x10^4$ cells/ml were incubated in Dulbecco's modified Eagle's medium containing 20 μM DHE (Vigorous Biotechnology Beijing Co., Ltd., Beijing, China; http://www.bioon.com.cn/show/reagent_88470_c0_p2.html.) at 37˚C for 10 min. Following loading DHE into the cells, the plate was mounted on a fluorescence microscope (x100 magnification, Nikon E-600), and fluorescence images were captured with a digital charge-coupled device camera (Roper Scientific RTE/CCD-1300-Y/HS) controlled by MetaMorph Image-analysis software version 4.01 (Universal Imaging, Inc., Bedford Hills, NY, USA). The Eth-DNA fluorescence was monitored at 490 nm excitation and 610 nm emission.

Western blot analysis. Cells were washed with ice-cold PBS twice. Lysis buffer (25 Mm Tris-HCl, Ph 7.4, 25 Mm NaCl, 0.5 Mm EDTA, 1 Mm sodium orthovanadate, 10 Mm NaF, 25 Mm β-glycerophosphate, 10 Mm sodium pyrophosphate, 0.2 Mm sodium molybdate, 10 mg/ml aprotinin, 2 Mm phenylmethylsulfonyl fluoride and 1% Triton X-100) was added to the cells, which were subjected to lysis by sonication for 60 sec on ice. The lysates were treated by centrifugation for 10 min at 12,000 x g at 4˚C, and the protein concentration was determined with a BCA protein concentration assay (Pierce; Thermo Fisher Scientific, Inc.). Equal amounts of protein (30 μg) were separated on 10-12.5% SDS-PAGE gels, electrophoretically transferred to polyvinylidene difluoride membranes with transfer buffer (25 mM Tris, 250 mM glycine and 10% methanol), the membranes were blocked with Western Blocking Buffer (cat. no. SW3010; Solarbio Life Sciences, China) at room temperature for 1 h. Probed with primary antibodies at 4˚C for 8 h, then horseradish peroxidase-conjugated secondary antibodies (Goat anti-rabbit IgG, HRP-linked Antibody, 1:1,000 dilution; cat. no. 7074; Cell Signaling Technology Inc., Danvers, MA, USA) at room temperature for 1 h. Immunoblots were detected using an ECL Prime Western Blotting Detection Reagent (GE Healthcare Life Sciences, Little Chalfont, UK), according to the manufacturer's protocol, autoradiography and recorded on film. Quantification was performed using ImageJ software version 1.45S (National institutes of Health, Bethesda, MD, USA). The primary antibodies used included: Rabbit anti-β-actin (1:5,000 dilution; cat. no. A2066; Sigma-Aldrich; Merck KGaA), γ-H2AX (ser139) (cat. no. 05-636-AF488; EMD Millipore) (1:2,000 dilution), cyclin dependent kinase 1 (CDK1; 1:5,000 dilution; cat. no. PLA0287; Sigma-Aldrich; Merck KGaA), checkpoint kinase 1 (CHK1; 1:500; cat. no. SAB4500207; Sigma-Aldrich; Merck KGaA), RAD51 recombinase (Rad51; dilution 1:500; cat. no. SAB2101936; Sigma-Aldrich; Merck KGaA), Ku70 (1:1,000 dilution; cat. no. 4104; Cell Signaling Technology Inc., Danvers, MA, USA) and Ku80 (1:1,000 dilution; cat. no. 2753; Cell Signaling Technology Inc.), B-cell lymphoma (Bcl-2; 1:5,000 dilution; cat. no. SAB4500003; Sigma-Aldrich; Merck KGaA), Bcl-2-associated X (Bax; 1:500 dilution; cat. no. SAB4502546; Sigma-Aldrich; Merck KGaA), BH3 interacting domain death agonist (Bid; 1:500 dilution; cat. no. SAB3500353; Sigma-Aldrich; Merck KGaA) and Caspase-9 (1:500 dilution; cat. no. 9502; Cell Signaling Technology Inc.), hypoxia inducible factor-1α (HIF-1α; 1:2,000 dilution; cat. no. SAB1405933; Sigma-Aldrich; Merck KGaA), glucose transporter 1 (GLUT1; 1:1,000 dilution; cat. no. SAB4502803; Sigma-Aldrich; Merck KGaA), c-Myc (1:1,000 dilution; cat. no. 13987; Cell Signaling Technology Inc.) and pyruvate kinase M2 (PKM2; 1:1,000; cat. no. 4053; Cell Signaling Technology Inc.).

Statistical analysis. All the experiments were repeated ≥3 times. Statistical analysis was performed with GraphPad Prism 5.0 Software (GraphPad Software, Inc., La Jolla, CA, USA). Data are presented as the mean ± SEM. $P \leq 0.05$ was considered to indicate a statistically significant difference. Cell cycle data were analyzed by two-way analysis of variance with dose and time point as independent variables, with Tukey's honestly significant difference (Tukey's HSD) as post-hoc test.

Results

ROS production in the cells following irradiation. Cells were incubated with DHE for 10 min after incremental doses of irradiation were administered. Red fluorescence produced by the formation and binding of ethidium (Eth) from DHE represents ROS production. The typical fluorescence microscopic images recorded at 10 min after incubation of DHE with different irradiation doses present maximal ROS-induced Eth-DNA red fluorescence. Red fluorescence of cells following irradiation, indicating production of ROS, was increased with a greater X-ray irradiation dose. As illustrated in Fig. 1, the ROS production in cells following irradiation was increased, and increased at increased doses. However, the fluorescence intensity demonstrated that there was no significant difference in ROS production between the 2 and 4 Gy groups.

Radiation-induced DNA damage. DNA double-strand breaks (DSBs) are induced directly by ionizing energy or indirectly by secondary radicals mediated by ROS (11). Phosphorylation of H2AX at Ser 139 (γ-H2AX) is the most sensitive marker used to detect DNA damage (12,13). In the present experiment,

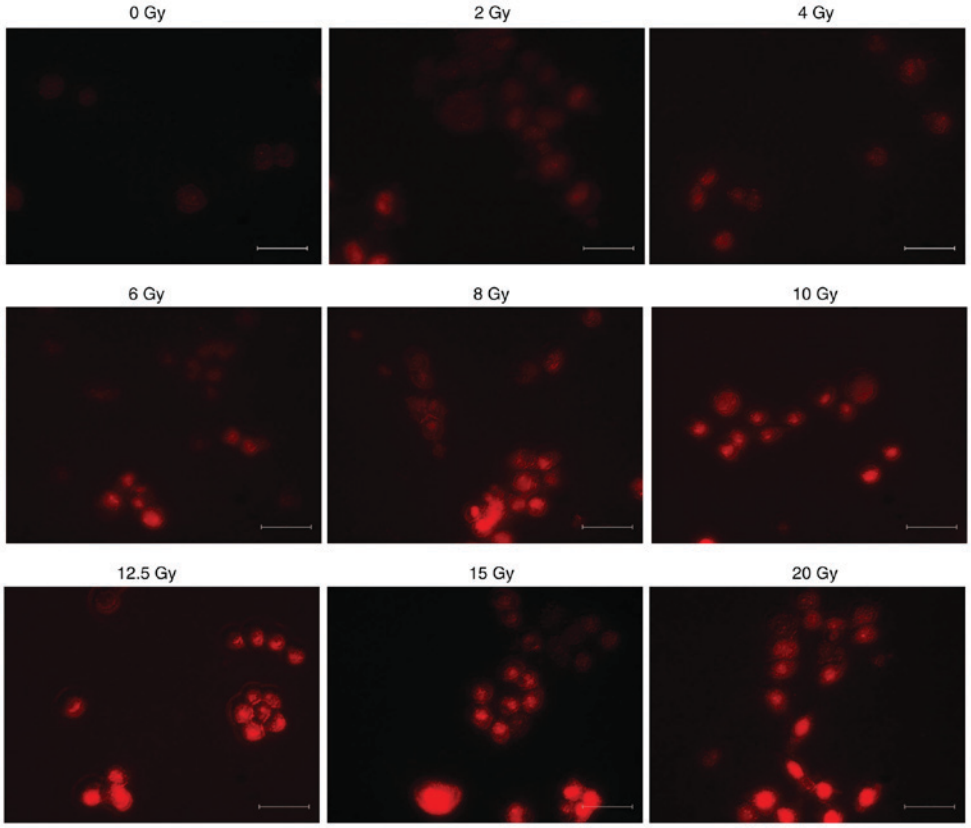

Figure 1. ROS production in the cells following irradiation. The formation of ethidium from dihydroethidium produced red fluorescence, which represents ROS production. A clear dose-dependent increase in ROS production was detected following X-irradiation. Scale bar, 100 μm. ROS, reactive oxygen species.

γ-H2AX was used as a marker of radiation-induced DNA DSBs.

To examine the dose-effect of radiation, DNA DSBs were visualized using immunofluorescent staining for γ-H2AX foci at 15 min after irradiation. Representative images of the γ-H2AX foci in HeLa cells were depicted in Fig. 2A. γ-H2AX was stained with green fluorescence (FITC), indicating that DSBs merged with the nucleus stained with red fluorescence (PI). A clear dose-dependent induction of the γ-H2AX foci was observed and was associated with the presence of DSBs. The expression of γ-H2AX at the protein level was detected by western blot analysis. The results of western blot analysis demonstrated that the expression of γ-H2AX increased following irradiation (Fig. 2B).

Cell cycle and cell proliferation following irradiation. Radiation-induced cell cycle changes were analyzed by flow cytometry at 0, 6, 12, 18, 24, 30, 36, 42 and 48 h after X-irradiation using PI staining. The primary results are depicted in Fig. 3A. The change trend of S-phase under different doses of irradiation was similar, within the 24 h following irradiation, the S-phase of cells with different dose were decreased gradually; and 30 h following irradiation, the change of S-phase exhibited a gradual increase. Following irradiation, a decrease trend of G1-phase was exhibited in HeLa cells, the higher the irradiation dose received, the greater the tendency of G1 phase reduction. Correspondingly, a significant increase in the number of HeLa cells in the G2/M-phase was observed following irradiation, indicative of DNA damage repair following irradiation (14,15). An increased dose of irradiation resulted in a greater G2/M delay. Cell cycling distribution returned to normal within 24 h after 2 Gy irradiation. The cells exposed to 4, 6 and 8 Gy returned to a normal cell cycle within 36 h, and cells exposed to 10 Gy returned to a normal cell cycle within 48 h. The cell cycle did not return to normal levels within 48 h when the radiation dose was >10 Gy (Fig. 3A). The expression of cell cycle-associated protein CDK1 markedly decreased following various doses of irradiation and the expression of CHK1 increased following irradiation. Variations in CDK1 and CHK1 were consistent with the accumulation of G2/M-phase cells (Fig. 3B).

Cell proliferation was detected by CCK-8 assays. The results represent the survival curves of HeLa cells exposed to the different doses of X-irradiation (Fig. 3C). The proliferation ability of cells irradiated with X-rays decreased with increasing doses.

Mitochondrial membrane potential and apoptosis following irradiation. Decrease in the mitochondrial membrane potential is an important signal of apoptosis in its early stage (16). The decrease in red fluorescence combined with the increase in green fluorescence indicated a loss of mitochondrial membrane potential, as depicted in Fig. 4. Compared with the cells without irradiation (0 Gy), the mitochondrial membrane potential of HeLa cells decreased following irradiation, and decreased at increased doses. The change of fluorescence also demonstrated that there was similar change of mitochondrial membrane potential between the 4 and 2 Gy groups. A

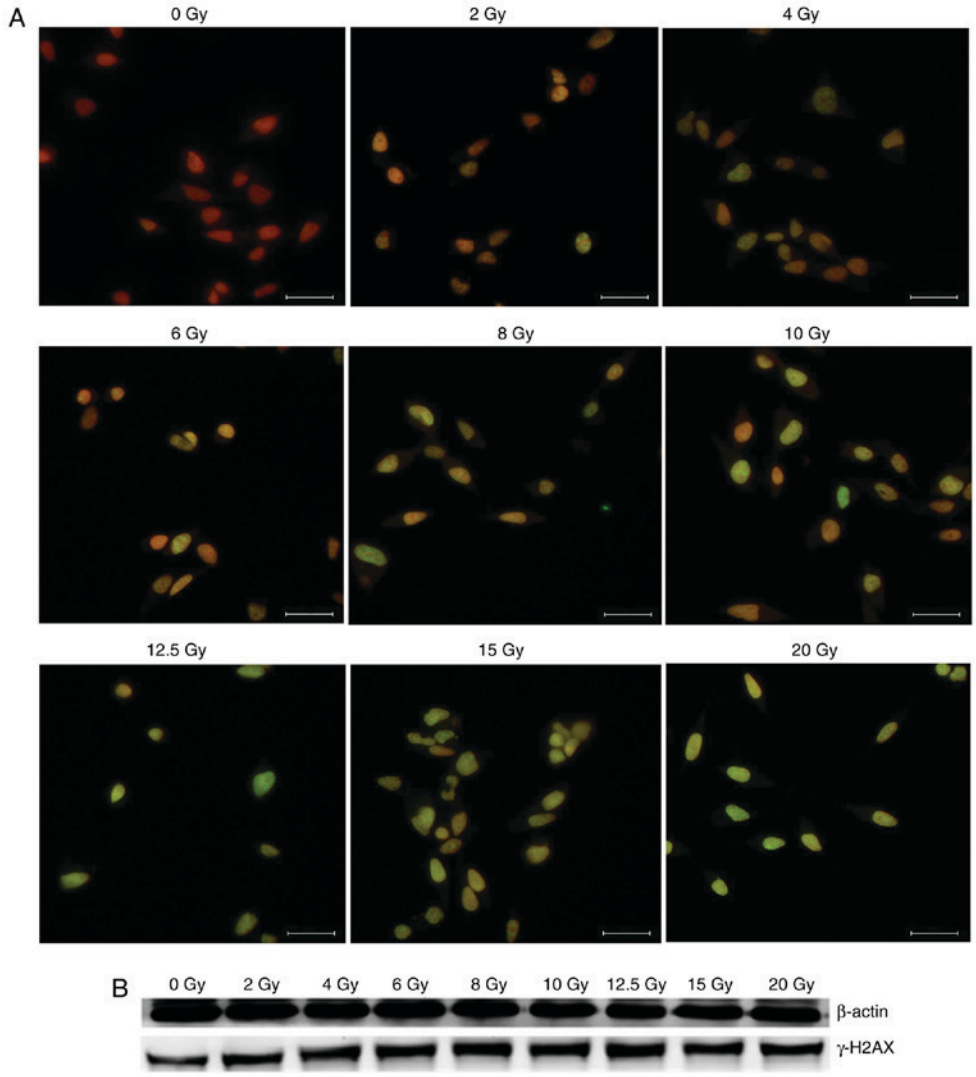

Figure 2. Radiation-induced DNA damage. (A) DNA double-strand breaks were visualized with immunofluorescent staining for γ-H2AX foci. γ-H2AX stained with green fluorescence (fluorescein isothiocyanate) reflects DSBs and merged with nucleus stained with red fluorescence (propidium iodide). Significant dose-dependent increase in foci number was detected following X-irradiation in HeLa cells. Scale bar, 100 μm. (B) Results of western blot analysis demonstrated the expression of γ-H2AX was increased following irradiation. γ-H2AX, phosphorylated histone H2AX.

dose-dependent decrease in mitochondrial membrane potential (MMP) was observed in cells irradiated at doses >4 Gy.

Further investigation of the dose response of apoptosis was performed by harvesting cells at 48 and 72 h after irradiation, staining with Annexin V-fluorescein isothiocyanate and PI, and analysis using a flow cytometer. It was determined that the proportion of apoptotic cells at 72 h after irradiation was increased, compared with the same dose at 48 h following irradiation (Fig. 5). Additionally, 48 and 72 h after irradiation have the identical change tendencies of apoptotic cells with different irradiation doses, a dose-dependent increase in the percentage of apoptotic cells was observed 48 and 72 h following irradiation. The results of the apoptosis assay indicated an increase in the percentage of apoptotic cells following irradiation (Fig. 5) The radio of apoptotic cells of two groups with adjacent doses were compared with each other. Except 2 and 4 Gy groups, the difference in the percentage of apoptotic cells between other adjacent two groups were significant; however, the difference in the percentage of apoptotic cells between the 2 and 4 Gy groups was not significant.

DNA damage repair- and apoptosis-associated proteins following irradiation. The expression of DNA damage-associated proteins was detected by western blot analysis (Fig. 6A). The expression of Rad51, which participates in homologous recombination (HR) repair (17), was markedly increased following irradiation, and the expression in the 2, 8 and 10 Gy groups was reduced, compared with the other groups. Generally, the expression of Ku70 and Ku80, which serve a notable role in Non-Homologous Endjoining (NHEJ) (18), were also increased following irradiation. Furthermore, levels of Ku70 in the 2, 8, 10, 12.5, 15 and 20 Gy groups, and Ku80 in the 6 and 8 Gy groups were markedly reduced, compared with the other groups. As reported, HR repair occurs in the S and G2-phases; however, NHEJ occurs throughout all phases of the cell cycle (19,20). Combined with the results of these two primary repair pathways, it may be concluded that for HeLa cells cultured *in vitro*, the DNA damage repair capability in the groups of 2, 6, 8 and 10 Gy were reduced, compared with the other groups, following irradiation.

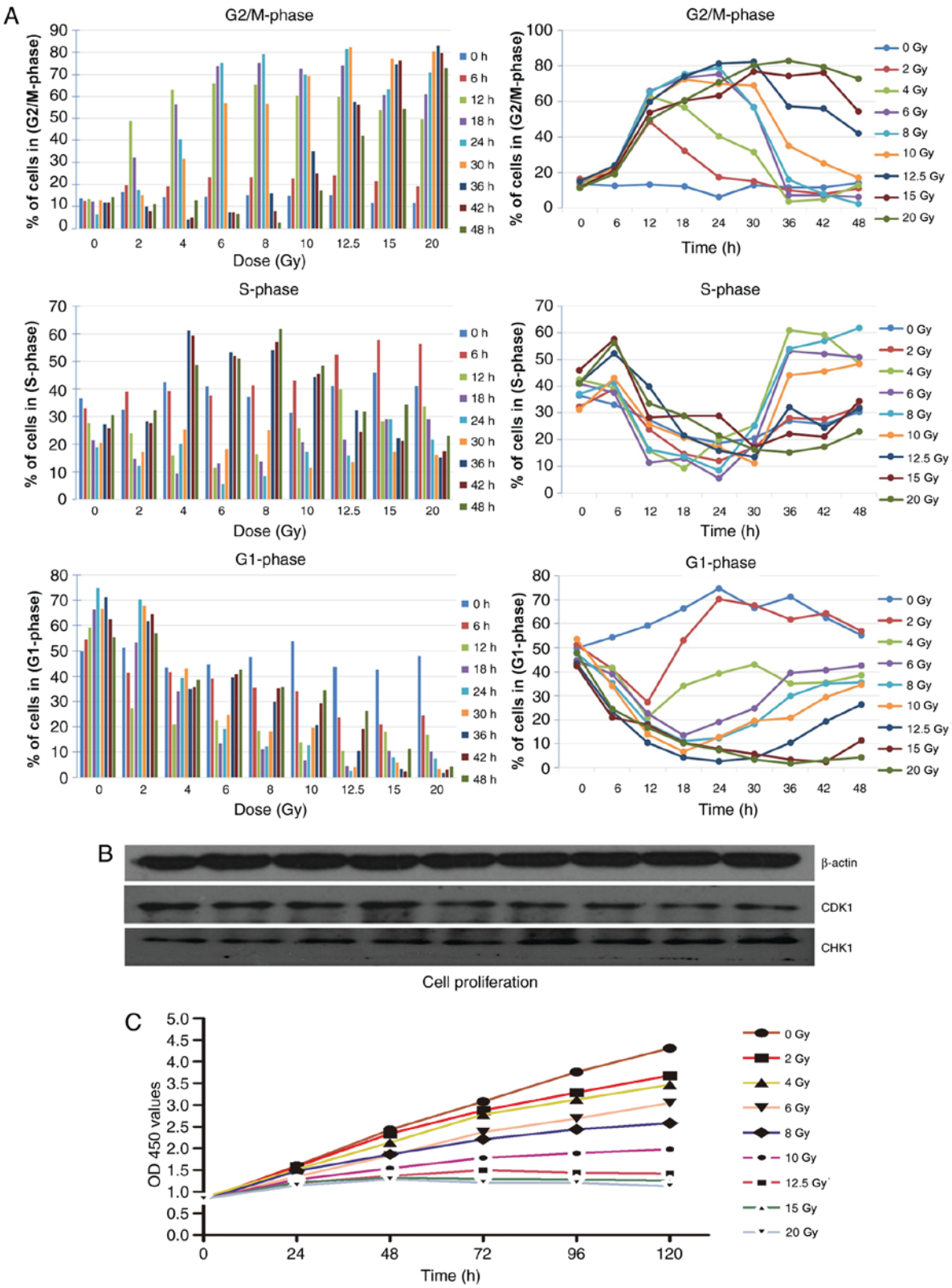

Figure 3. Cell cycle following irradiation. (A) Cell cycle (G1, S and G2/M) changes were analyzed by flow cytometry at 0, 6, 12, 18, 24, 30, 36, 42 and 48 h after X-ray irradiation using propidium iodide staining. Irradiation of HeLa cells resulted in a notable increase of cells in the G2/M-phase. (B) Results of western blot analysis demonstrated the level of CDK1 and CHK1 in cells following irradiation, the expression of CDK1 markedly decreased following various doses of irradiation and the expression of CHK1 increased following irradiation. (C) Cell proliferation was detected using Cell Counting Kit-8 assays in cells following irradiation. CDK1, cyclin dependent kinase 1; CHK1, checkpoint kinase 1; OD, optical density.

Expression of apoptosis-associated proteins was detected by western blot analysis (Fig. 6B). Compared with the 0 Gy group, the expression of the Bcl-2 apoptosis suppression protein was markedly decreased following different doses of irradiation. However, pro-apoptosis protein Bax increased following irradiation, but the expression of Bax in the 6, 8,

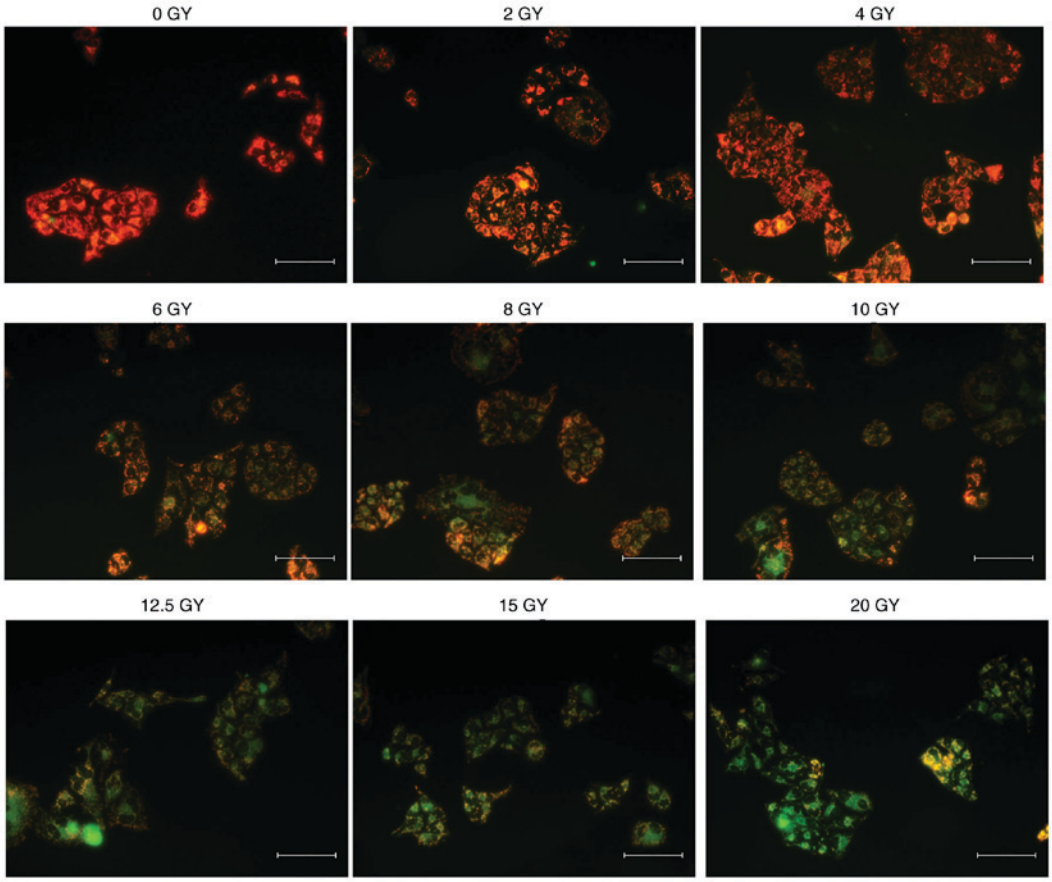

Figure 4. Mitochondrial membrane potential following irradiation. The change of mitochondrial membrane potential in cells following irradiation. The images demonstrated depolarization of the mitochondrial membrane potential indicated by a decrease of the red fluorescence combined with an increase of the green fluorescence. Scale bar, 100 μm.

10 and 12.5 Gy groups was notably increased, compared with the other groups. Additionally, the apoptosis-associated proteins Bid was elevated following irradiation, compared with the control group (0 Gy). The expression of Bid in the 6, 8 and 10 Gy groups were increased, compared with the other groups. The expression of procaspase-9 and cleaved Caspase-9 was increased in the 2, 4, 6 and 8 groups, however, a downward trend was observed following 6 Gy. Generally, increased expression levels of apoptosis-associated proteins were determined in the 2, 6, 8 and 10 Gy groups.

Aerobic glycolysis metabolic following irradiation. Given that radiation may alter tumor glucose metabolism through the aerobic glycolysis metabolic pathway (21,22), the present study detected changes associated with aerobic glycolysis following irradiation that may alter the energy of cancer cells.

Compared with 0 Gy, the results of the western blot analysis (Fig. 6C) demonstrated an increasing trend in the expression of HIF-1α following irradiation in a dose-dependent manner, and a similar trend was observed in the expression of c-Myc; however, the expression of HIF-1α and c-Myc in the 4, 6, 12.5 and 20 Gy were higher than the other groups. GLUT1 is one of most important glucose transporters in cancer cells (23). The expression level of GLUT1 was markedly increased following irradiation, but was reduced in the 12.5, 15 and 20 Gy groups. HIF-1α, c-Myc and GLUT1 serve an important role in promoting glycolysis and glucose uptake (24). The expression of PKM2 in the groups with irradiation doses from 2-10 Gy were reduced, compared with the other groups, indicating that the levels of glycolysis in these groups may be reduced, compared with the other groups.

Discussion

In recent years, SBRT and stereotactic radiation surgery have been increasingly used to treat cancer (25). SBRT is a novel radiotherapy technique, which has high locoregional control rates (2). The rapid development of SBRT was primarily due to the advantage that one or a few fractions of high-dose ionizing radiation may be administered with high-target accuracy and rapid dose-falloff gradients (8,26). A notable cancer control result with limited complications can be obtained.

Ionizing radiation is one of the most important inducers of cellular damage. Indicators of cellular damage detection include identification of DNA damage, such as through the detection of γ-H2AX foci, DNA damage repair and cell survival. Cellular damage indicators may also include other effects, including cell cycle alterations, glycolysis effect and cell apoptosis (11,12). Direct and indirect effects may be induced by cellular exposure to X-ray radiation (27). The DNA damage induced by irradiation could result in direct effects, whereas indirect biological effects are associated with ROS generated by radiolysis and subsequent reactions (28). DNA is more susceptible to being attacked by ROS generated by low

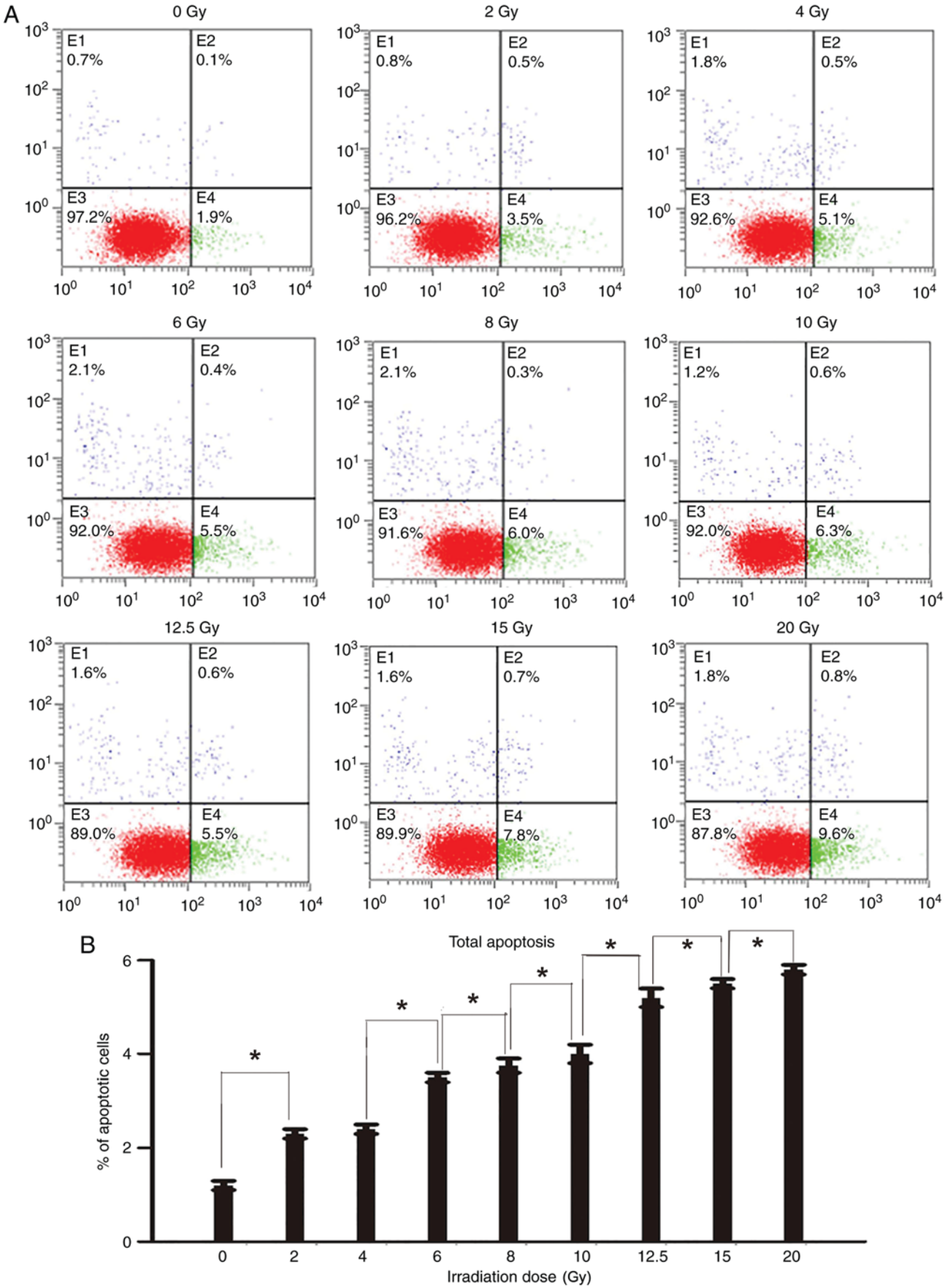

Figure 5. Apoptosis of cells following irradiation. (A) The apoptotic cells at 48 h after irradiation, stained with Annexin V-FITC and PI, were analyzed using a flow cytometer. Cells were classified into 4 subpopulations as follows: Viable cells (lower left), early apoptotic cells (lower right), cell fragments and damaged cells (upper left), and late apoptotic cells (upper right). (B) The percentage of apoptotic cells at 48 h after irradiation with different irradiation doses (lower right and upper right). The radio of apoptotic cells of two groups with adjacent doses were compared with each other. Except 2 and 4 Gy groups (difference between the 2 and 4 Gy groups was not significant), the difference in the percentage of apoptotic cells between other adjacent two groups were significant $^{*}P<0.05$.

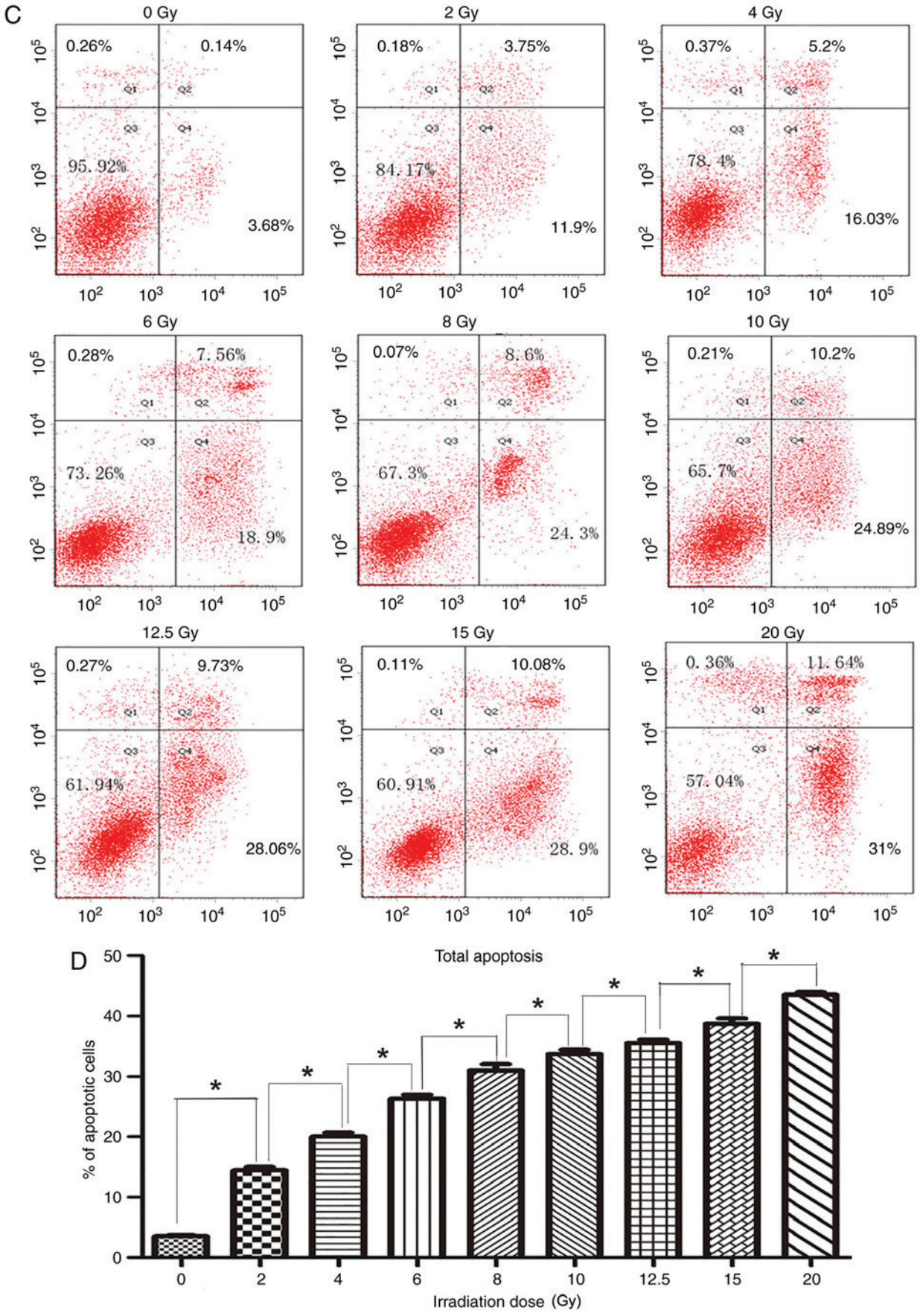

Figure 5. Continued. (C) The apoptotic cells at 72 h after irradiation, stained with Annexin V-FITC and PI, were analyzed using a flow cytometer. Cells were classified into 4 subpopulations as follows: Viable cells (lower left), early apoptotic cells (lower right), cell fragments and damaged cells (upper left), and late apoptotic cells (upper right). (D) The percentage of apoptotic cells at 72 h after irradiation with different irradiation doses (lower right and upper right). The radio of apoptotic cells of two groups with adjacent doses were compared with each other. Except 2 and 4 Gy groups (difference between the 2 and 4 Gy groups was not significant), the difference in the percentage of apoptotic cells between other adjacent two groups were significant *P<0.05. FITC, fluorescein isothiocyanate; PI, propidium iodide.

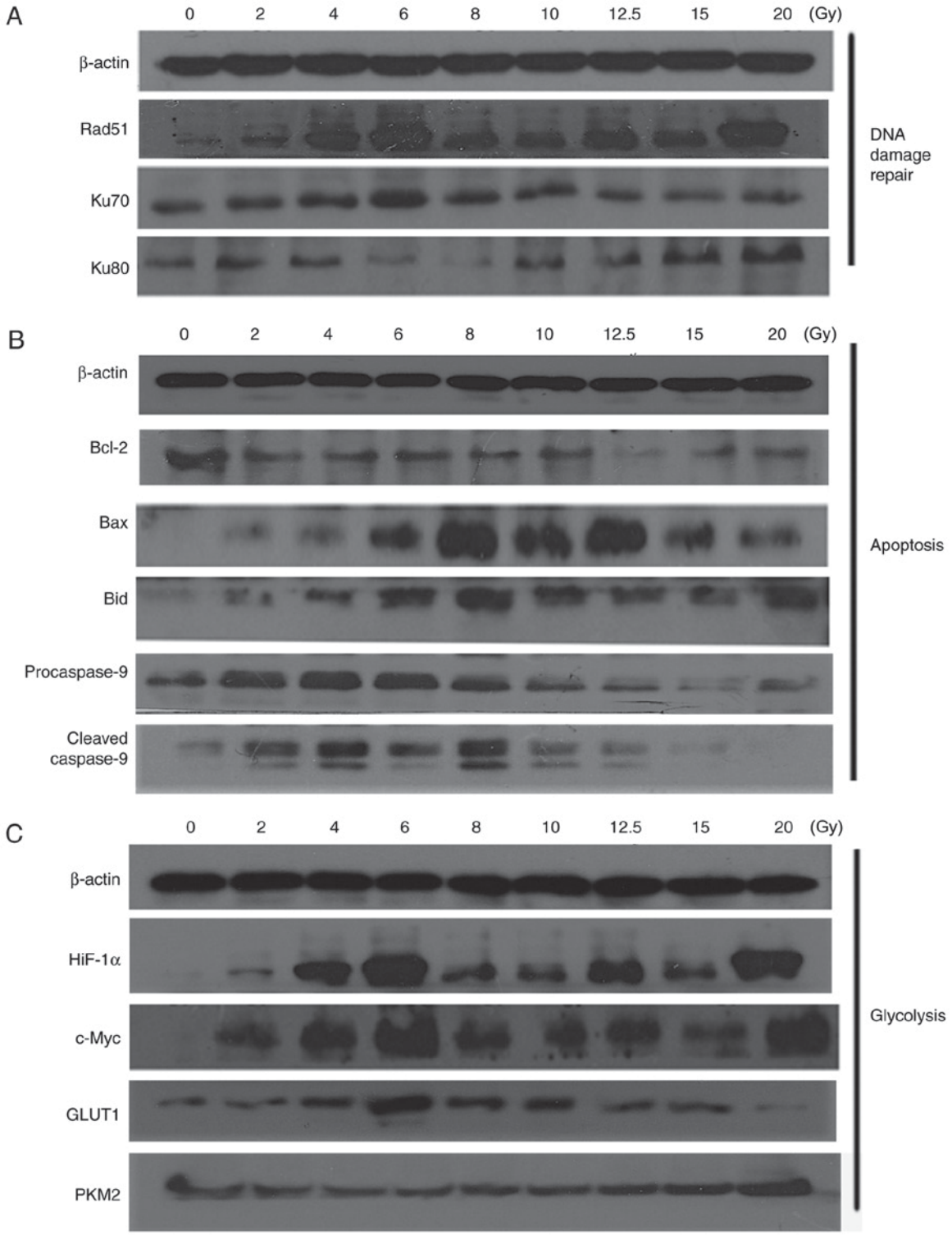

Figure 6. Proteins associated with DNA damage repair, apoptosis and glycolysis following irradiation. (A) Results of western blot analysis demonstrated the expression of proteins associated with DNA damage repair following different doses of irradiation. (B) Results of western blot analysis indicated the expression of proteins associated with apoptosis following different doses of irradiation. (C) Results of western blot analysis demonstrated the expression of proteins associated with glycolysis following different doses of irradiation. Bcl-2, B-cell lymphoma-2; Bax, Bcl-2-associated X; Bid, BH3 interacting domain death agonist; HiF-1α, hypoxia inducible factor-1α; GLUT1, glucose transporter 1; PKM2, pyruvate kinase M2.

LET radiation (28). The ROS produced during irradiation can oxidize bases, and induce single-strand breaks (SSBs) and DNA double-strand breaks (DSBs) (29). In the present experiment, the production of ROS and γ-H2AX foci exhibited identical variation tendencies in HeLa cells following different X-ray irradiation doses, the production of ROS and γ-H2AX foci in cells following irradiation were all increased, and increased at increased doses, this suggests that ROS production has a critical relationship with DNA damage.

There are two molecularly distinct G2/M checkpoints that may be identified. The first one occurs early, is very transient, and is dose independent; in contrast, the second one is 'late'

G2/M accumulation, typically assessed by propidium iodide staining, the late G2/M accumulation has an important character which is ATM independent and dose-dependent. The late one can be used to represent the accumulation of cells in early stages of the cell cycle following exposure to radiation (30). The G2/M arrest detected in the present study indicates late G2/M accumulation, which is dose-dependent, and this character of late G2/M accumulation which is dose-dependent combined with the present results, the G2/M delay in cells following irradiation was increased at increased irradiation doses. In contrast, early G2/M arrest is transient, ATM dependent and dose-independent. Additionally, it can be induced in the early period following exposure to ionizing radiation (31,32). G2/M delay in tumor cells following irradiation may provide sufficient time for repair processes and is important for ensuring cell survival following sub-lethal DNA damage in cells (32). Considering HR repair occurs in the S and G2-phases and G2/M delay following irradiation may provide sufficient time for repair (17,32), the G2/M-phase arrest is important for DNA damage repair following irradiation (14,15). The present results demonstrated that the cell cycle returned to the normal range within 48 h after irradiation with doses <10 Gy, while the cell cycle could not return to normal level within 48 h with doses ≥10 Gy. This phenomenon may indicate that the DNA repair ability was not sufficient to repair DNA damage induced by irradiation when the dose exceeded 10 Gy. Apoptotic cells were detected at 48 and 72 h after irradiation for each radiation dose. The proportion of apoptotic cells at 72 h after irradiation was increased, compared with at 48 h. Taken together these results suggest that DNA damage that cannot be repaired within 48 h after irradiation may have resulted in the number of apoptotic cells at 72 h after irradiation being increased, compared with that at 48 h.

DSBs are detected by detecting γ-H2AX activation in cells (33). Repair enzymes are attracted and gathered to the damaged points of DNA as cells go into cell cycle arrest, producing sufficient time for cellular repair (13). There are two pathways for DSB repair that have been identified in mammalian cells: HR and NHEJ, NHEJ repair occurs in all phases of the cell cycle, but primarily in the G1 phase, whereas HR generally occurs during the S/G2 phases (27,34,35). Additionally, previous studies indicated that while HR has the capacity to repair damage in G2 phase, NHEJ is the primary repair pathway in the G2 and G1 phases with 75-85% of irradiation-induced DSBs undergoing repair via NHEJ in mammalian cells (19,20,36).

The NHEJ pathway is the most important pathway to repair DSBs induced by radiation (37). The major molecule in this pathway is the Ku70/80 heterodimer (KU) (18). To activate the NHEJ pathway, the KU binds to blunt or near-blunt DNA ends. Subsequently, the recruitment and activation of DNA-dependent protein kinase catalytic subunit, that depends on DSB-bound KU, triggers a wide range of downstream signaling cascades that coordinate the repair processes (18). Rad51 is the key molecule in HR (17) and interacts with the BRCA2 DNA repair associated molecule in the process of combining the two homologous DNA strands (38,39).

If DNA damage cannot be adequately repaired, cells progress towards apoptosis and/or necrosis (36). A decrease in the mitochondrial membrane potential is an important initiator of apoptosis in its early stages (15). The change in the mitochondrial membrane potential of cells exposed to radiation in the present study indicated that the mitochondrial apoptotic pathway was activated, but the change in the 2 and 4 Gy groups were similar, and a clear dose-dependent decrease of MMP was observed in cells administered with an irradiation dose >4 Gy. Bcl-2 family proteins, including the pro-apoptosis protein Bax and the apoptosis-inhibitor Bcl-2, regulate cell apoptosis. Characteristic morphological changes in cells and DNA that are associated with apoptosis are primarily associated with the activation of cysteine proteinases (caspases) (40). Cell apoptosis through the mitochondrial-dependent pathway is accompanied by the release of cytochrome *c*, followed by activation of the caspase cascade (41). The present results demonstrated that the 2-10 Gy groups achieved an improved result with a pro-apoptosis effect.

Toxicity to normal tissue and other cellular effects, including hypoxia and glycolysis, are limitations on the efficacy of radiotherapy in solid tumor types (42). Glycolysis is an advantageous metabolic pathway for cancer cells, including adaptation to hypoxia and resistance to mitochondria-mediated apoptosis (23,43). A number of studies have observed an increase in the activity of the HIF-1α transcription factor following radiation, which regulates metabolism, invasion and protection against oxidative stress (24,44). Numerous glycolytic enzymes are regulated by HIF-1α, including lactate dehydrogenase and PKM2, its upregulation stimulates glucose uptake and glycolysis in cells (24). Previous reports have identified the glycolysis effect to be implicated in resistance to cytotoxic stress, including that caused by ionizing radiation and chemotherapy (21,45). The present data indicated that the expression of HIF-1α and c-Myc markedly increased following irradiation, serving an important role in promoting glycolysis. However, the level of GLUT1 in the 12.5, 15 and 20 Gy groups indicated a diminished ability for glucose uptake in these groups. These results were consistent with overall cell cycle changes. In the present study, cell cycle progression did not return to normal level within 48 h after irradiation with doses ≥10 Gy, which may indicate that DNA damage exceeded the capacity of repair mechanisms. Cells may then progress towards apoptosis and necrosis. Aerobic glycolysis can be induced with the expression of PKM2, which is a regulator of glycolysis (46,47). The glycolysis effect was reduced in the 2-10 Gy dose groups. Since these results were gathered from cancer cells cultured *in vitro*, further corroboration is required using *in vivo* experiments.

In conclusion, in tumor cells, X-ray irradiation is known to induce DNA DSBs, ROS, cellular apoptosis and G2/M phase arrest. Compared with 2 Gy of radiation/fraction, a 4 Gy/fraction dose did not demonstrate evident advantages in common biological effects. Considering DNA damage repair and the apoptotic mechanism of cells at the molecular and cellular levels following different dose of irradiation, it may be concluded that 2, 6, 8 and 10 Gy may be the optimal fractional doses with notable biological responses.

Acknowledgements

The authors would like to thank Dr. Ji Chen who worked in Department of Radiation and Medical Oncology, Zhongnan

Hospital Affiliated to Wuhan University for guiding them in the use of the irradiation facility.

Funding

This research was supported by National Natural Science Foundation of China (grant no. 81472799).

Availability of data and materials

The datasets used and/or analyzed during the present study are available from the corresponding author on reasonable request.

Authors' contributions

YunZ and FZ designed the experiments. ZM, HZ and YafZ performed the experiments. RL, YL and ZH analyzed the data. HZ wrote the paper. YunZ edited the manuscript.

Ethics approval and consent to participate

Not applicable.

Patient consent for publication

Not applicable.

Competing interests

The authors declare that they have no competing interests.

References

1. Bergonié J and Tribondeau L: Interpretation of some results from radiotherapy and an attempt to determine a rational treatment technique. 1906. Yale J Biol Med 76: 181-182, 2003.
2. Timmerman RD and Kavanagh BD: Stereotactic body radiation therapy. Curr Probl Cancer 29: 120-157, 2005.
3. Kim MS, Kim W, Park IH, Kim HJ, Lee E, Jung JH, Cho LC and Song CW: Radiobiological mechanisms of stereotactic body radiation therapy and stereotactic radiation surgery. Radiat Oncol J 33: 265-275, 2015.
4. Tsang MW: Stereotactic body radiotherapy: Current strategies and future development. J Thorac Dis 8 (Suppl 6): S517-S527, 2016.
5. Sapkaroski D, Osborne C and Knight KA: A review of stereotactic body radiotherapy-is volumetric modulated arc therapy the answer? J Med Radiat Sci 62: 142-151, 2015.
6. Kavanagh BD, Timmerman RD, Benedict SH, Wu Q, Schefter TE, Stuhr K, McCourt S, Newman F, Cardinale RM and Gaspar LF: How should we describe the radioblologic effect of extracranial stereotactic radlosurgery: Equivalent uniform dose or tumor control probability? Med Phys 30: 321-324, 2003.
7. Hof H, Herfarth KK, Münter M, Hoess A, Motsch J, Wannenmacher M and Debus JJ: Stereotactic single-dose radiotherapy of stage I non-small-cell lung cancer (NSCLC). Int J Radiat Oncol Biol Phys 56: 335-341, 2003.
8. Timmerman R, Papiez L and Suntharalingam M: Extracranial stereotactic radiation delivery: Expansion of technology beyond the brain. Technol Cancer Res Treat 2: 153-160, 2003.
9. Potters L, Steinberg M, Rose C, Timmerman R, Ryu S, Hevezi JM, Welsh J, Mehta M, Larson DA, Janjan NA and American Society for Therapeutic Radiology and Oncology; American College of Radiology: American society for therapeutic radiology and oncology and american college of radiology practice guideline for the performance of stereotactic body radiation therapy. Int J Radiat Oncol Biol Phys 60: 1026-1032, 2004.
10. Timmerman RD, Forster KM and Chinsoo Cho L: Extracranial stereotactic radiation delivery. Semin Radiat Oncol 15: 202-207, 2005.
11. Barilla J, Lokajíček M, Pisaková H and Simr P: Analytical model of chemical phase and formation of DSB in chromosomes by ionizing radiation. Australas Phys Eng Sci Med 36: 11-17, 2013.
12. Sharma A, Singh K and Almasan A: Histone H2AX phosphorylation: A marker for DNA damage. Methods Mol Biol 920: 613-626, 2012.
13. Tanaka T, Halicka D, Traganos F and Darzynkiewicz Z: Cytometric analysis of DNA damage: Phosphorylation of histone H2AX as a marker of DNA double-strand breaks (DSBs). Methods Mol Biol 523: 161-168, 2009.
14. Stark GR and Taylor WR: Control of the G2/M transition. Mol Biotechnol 32: 227-248, 2006.
15. Yan Y, Black CP and Cowan KH: Irradiation-induced G2/M checkpoint response requires ERK1/2 activation. Oncogene 26: 4689-4698, 2007.
16. Hu D and Kipps TJ: Reduction in mitochondrial membrane potential is an early event in Fas-independent CTL-mediated apoptosis. Cell Immunol 195: 43-52, 1999.
17. Liu Q, Jiang H, Liu Z, Wang Y, Zhao M, Hao C, Feng S, Guo H, Xu B, Yang Q, *et al*: Berberine radiosensitizes human esophageal cancer cells by downregulating homologous recombination repair protein RAD51. PLoS One 6: e23427, 2011.
18. Dynan WS and Yoo S: Interaction of Ku protein and DNA-dependent protein kinase catalytic subunit with nucleic acids. Nucleic Acids Res 26: 1551-1559, 1998.
19. Orthwein A, Fradet-Turcotte A, Noordermeer SM, Canny MD, Brun CM, Strecker J, Escribano-Diaz C and Durocher D: Mitosis inhibits DNA double-strand break repair to guard against telomere fusions. Science 344: 189-193, 2014.
20. Symington LS and Gautier J: Double-strand break end resection and repair pathway choice. Annu Rev Genet 45: 247-271, 2011.
21. Pitroda SP, Wakim BT, Sood RF, Beveridge MG, Beckett MA, MacDermed DM, Weichselbaum RR and Khodarev NN: STAT1-dependent expression of energy metabolic pathways links tumour growth and radioresistance to the Warburg effect. BMC Med 7: 68, 2009.
22. Khodarev NN, Beckett M, Labay E, Darga T, Roizman B and Weichselbaum RR: STAT1 is overexpressed in tumors selected for radioresistance and confers protection from radiation in transduced sensitive cells. Proc Natl Acad Sci USA 101: 1714-1719, 2004.
23. Gatenby RA and Gillies RJ: Why do cancers have high aerobic glycolysis? Nat Rev Cancer 4: 891-899, 2004.
24. Kondoh H, Lleonart ME, Gil J, Wang J, Degan P, Peters G, Martinez D, Carnero A and Beach D: Glycolytic enzymes can modulate cellular life span. Cancer Res 65: 177-185, 2005.
25. Lo SS, Slotman BJ, Lock M, Nagata Y, Guckenberger M, Siva S, Foote M, Tan D, The BS, Mayr NA, *et al*: The development of stereotactic body radiotherapy in the past decade: A global perspective. Future Oncol 11: 2721-2733, 2015.
26. Potters L, Kavanagh B, Galvin JM, Hevezi JM, Janjan NA, Larson DA, Mehta MP, Ryu S, Steinberg M, Timmerman R, *et al*: American society for therapeutic radiology and oncology (ASTRO) and american college of radiology (ACR) practice guideline for the performance of stereotactic body radiation therapy. Int J Radiat Oncol Biol Phys 76: 326-332, 2010.
27. Borek C: Antioxidants and radiation therapy. J Nutr 134: 3207S-3209S, 2004.
28. Aparicio T, Baer R and Gautier J: DNA double-strand break repair pathway choice and cancer. DNA Repair (Amst) 19: 169-175, 2014.
29. Illner D and Scherthan H: Ionizing irradiation-induced radical stress stalls live meiotic chromosome movements by altering the actin cytoskeleton. Proc Natl Acad Sci USA 110: 16027-16032, 2013.
30. Xu B, Kim ST, Lim DS and Kastan MB: Two molecularly distinct G(2)/M checkpoints are induced by ionizing irradiation. Mol Cell Biol 22: 1049-1059, 2002.
31. Marples B, Wouters BG and Joiner MC: An association between the radiation-induced arrest of G2-phase cells and low-dose hyper-radiosensitivity: A plausible underlying mechanism? Radiat Res 160: 38-45, 2003.
32. Fingert HJ, Chang JD and Pardee AB: Cytotoxic, cell cycle, and chromosomal effects of methylxanthines in human tumor cells treated with alkylating agents. Cancer Res 46: 2463-2467, 1986.
33. Kinner A, Wu W, Staudt C and Iliakis G: Gamma-H2AX in recognition and signaling of DNA double-strand breaks in the context of chromatin. Nucleic Acids Res 36: 5678-5694, 2008.
34. Helleday T, Lo J, van Gent DC and Engelward BP: DNA double-strand break repair: From mechanistic understanding to cancer treatment. DNA Repair (Amst) 6: 923-935, 2007.

35. Rothkamm K, Krüger I, Thompson LH and Löbrich M: Pathways of DNA double-strand break repair during the mammalian cell cycle. Mol Cell Biol 23: 5706-5715, 2003.
36. Beucher A, Birraux J, Tchouandong L, Barton O, Shibata A, Conrad S, Goodarzi AA, Krempler A, Jeggo PA and Löbrich M: ATM and Artemis promote homologous recombination of radiation-induced DNA double-strand breaks in G2. EMBO J 28: 3413-3427, 2009.
37. Vandersickel V, Depuydt J, Van Bockstaele B, Perletti G, Philippe J, Thierens H and Vral A: Early increase of radiation-induced γH2AX foci in a human Ku70/80 knockdown cell line characterized by an enhanced radiosensitivity. J Radiat Res 51: 633-641, 2010.
38. Saydam O, Saydam N, Glauser DL, Pruschy M, Dinh-Van V, Hilbe M, Jacobs AH, Ackermann M and Fraefel C: HSV-1 amplicon-mediated post-transcriptional inhibition of Rad51 sensitizes human glioma cells to ionizing radiation. Gene Ther 14: 1143-1151, 2007.
39. Johnson RD and Jasin M: Sister chromatid gene conversion is a prominent double-strand break repair pathway in mammalian cells. EMBO J 19: 3398-3407, 2000.
40. Roos WP and Kaina B: DNA damage-induced cell death: From specific DNA lesions to the DNA damage response and apoptosis. Cancer Lett 332: 237-248, 2013.
41. Pardo FS, Su M and Borek C: Cyclin D1 induced apoptosis maintains the integrity of the G1/S checkpoint following ionizing radiation irradiation. Somat Cell Mol Genet 22: 135-144, 1996.
42. Brown JM, Diehn M and Loo BW Jr: Stereotactic ablative radiotherapy should be combined with a hypoxic cell radiosensitizer. Int J Radiat Oncol Biol Phys 78: 323-327, 2010.
43. Zimmermann KC, Bonzon C and Green DR: The machinery of programmed cell death. Pharmacol Ther 92: 57-70, 2001.
44. Semenza GL: Oxygen sensing, homeostasis, and disease. N Engl J Med 365: 537-547, 2011.
45. Kim JW and Dang CV: Cancer's molecular sweet tooth and the warburg effect. Cancer Res 66: 8927-8930, 2006.
46. Wang T, Marquardt C and Foker J: Aerobic glycolysis during lymphocyte proliferation. Nature 261: 702-705, 1976.
47. Christofk HR, Vander Heiden MG, Harris MH, Ramanathan A, Gerszten RE, Wei R, Fleming MD, Schreiber SL and Cantley LC: The M2 splice isoform of pyruvate kinase is important for cancer metabolism and tumour growth. Nature 452: 230-233, 2008.